Dislocation Network Formation and Coherency Loss around Gamma-Prime Precipitates in a Nickel-Base Superalloy

A. K. SINGH, N. LOUAT, and K. SADANANDA

A study of the loss of coherency suffered by gamma-prime precipitates after aging or through plastic deformation was carried out in a superalloy, IN 713C.* Selected aging treatments were employed so as to observe different stages of coherency loss. Examination using transmission electron microscopy reveals that itinerant or matrix dislocations, generated either by internal stresses (carbides, *etc.*) or through the usual processes of general plastic deformation, rearrange themselves by cross-slip and climb around gamma-prime precipitates to produce misfit dislocation networks. Along with the network formation, the precipitate morphology changes to maximize the misfit accommodation. The final dislocation and precipitate configurations are consistent with the Lasalmonie and Strudel model.

I. INTRODUCTION

NICKEL base superalloys are used extensively in gas turbine components. High volume fractions of ordered intermetallic precipitates of gamma-prime ($Ni_3(Al, Ti)$) with LI_2 structure essentially provide the strength for these alloys. Because of the small lattice misfit between the nickel-rich matrix, gamma, and the gamma-prime phases, the precipitates are coherent with (100) of the matrix parallel to (100) of the precipitates. In addition, they tend to form cuboidal precipitates with their faces aligned along cube directions. The degree of the lattice misfit, the difference in the elastic moduli of the matrix, and the precipitates and the anisotropy of these moduli are all important in determining the formation of this cuboidal configuration and the alignment of the precipitates. For the purpose of the present analysis, we consider the precipitates coherent because of the absence of any misfit dislocations. They become semicoherent with the reduction in the strain energy when misfit dislocations are formed.

In addition to the size and distribution of the precipitates, the nature of the interface between the precipitates and the matrix plays an important role in determining the strength of the alloy. Although the initial interfaces are fully coherent, misfit dislocations form readily with plastic deformation at high temperatures or with prolonged aging. Because of the technological importance, several studies[1,2,3] have been made of the role of the gamma-gamma prime interfaces and of the formation of semicoherent precipitates through the interactions of the mobile dislocations in the matrix with the precipitates.

From these studies it is now clear that a network of prismatic dislocation (having Burgers vectors of $a/2\langle 110\rangle$)[4,5] is formed at the interface of each precipitate during deformation. While it is recognized that they are related to the glide dislocations in the matrix, it is not clear how these glide dislocations form misfit dislocation networks of predominantly edge character around the gamma-prime precipitates. The objective of the present study is to examine the detailed process of the formation of this misfit dislocation network. Understanding of the misfit dislocation formation is important since strength of these alloys is intimately connected with the morphology of the precipitate and the nature of the precipitate-matrix interface, both being affected by the network formation. In particular, this network formation can reduce the strength of the alloy by decreasing the contribution from coherency stresses in the neighborhood of the precipitates.

This is a part of the extensive study to understand the role of the interfacial dislocations and their effect on the morphological stability of gamma-prime precipitates in nickel base superalloys. While the study was made using several cast gas turbine blade alloys such as IN 713C, B 1900, and IN 100, the results were not sensitive to the alloy composition. For the purpose of illustration we discuss the results with reference to alloy IN 713C.

II. EXPERIMENTAL PROCEDURES

Round bar cast specimens of the alloy IN 713C were obtained from a vendor. The nominal composition of the alloy is given in Table I.

Some of the specimens were cut and heat treated for microstructural analysis while others were machined for creep study. In order to follow the evolution of interfacial dislocation network, specimens were solutionized at 1225 °C, water quenched, and then heat treated at 1000 °C for different lengths of time. Thin foils for electron microscopy were prepared by the twin jet polishing method using a solution consisting of 250 cc of methyl alcohol, 150 cc of butanol, and 15 cc of perchloric acid at 70 volts and −50 °C. These foils were examined in JEOL 200 microscope operated at 200 kv using a double tilt goniometer in diffraction and imaging modes.

A. *Burgers Vector Analysis*

To analyze the dislocations at the interface of gamma and gamma-prime, the usual contrast experiments

*IN is a trademark of the INCO family of companies.

A. K. SINGH and N. LOUAT, Senior Scientists and On-Site Contract Employees at Naval Research Laboratory, are with Geo. Centers, Inc., 10903 Indian Head Highway, Fort Washington, MD 20744. K. SADANANDA is Head, Deformation and Failure Section, Physical Metallurgy Branch, Materials Science and Technology Division, Naval Research Laboratory, Washington, DC.

Manuscript submitted September 8, 1987.

Table I. Chemical Composition of Alloy 713C

Element	C	Cr	Mo	Nb	Ti	Al	B	Zr	Fe	Ni
Wt pct	0.12	12.5	4.2	2	0.8	6.1	0.012	0.10	2.5	bal.

($\bar{g}.\bar{b}$. method) were carried out. Since both the gamma and gamma-prime phases are cubic, the dislocation could be analyzed by choosing three **g** vectors as $11\bar{1}$, $1\bar{1}1$, $\bar{1}11$. These three **g** vectors can be found by tilting the (111) section of the foil. Two sets of examples of this technique for the determination of Burgers vector of interfacial dislocations are shown in Figures 1(a), (b), and (c) and Figures 2(a), (b), and (c). Micrographs (a), (b), and (c) of Figure 1 show the

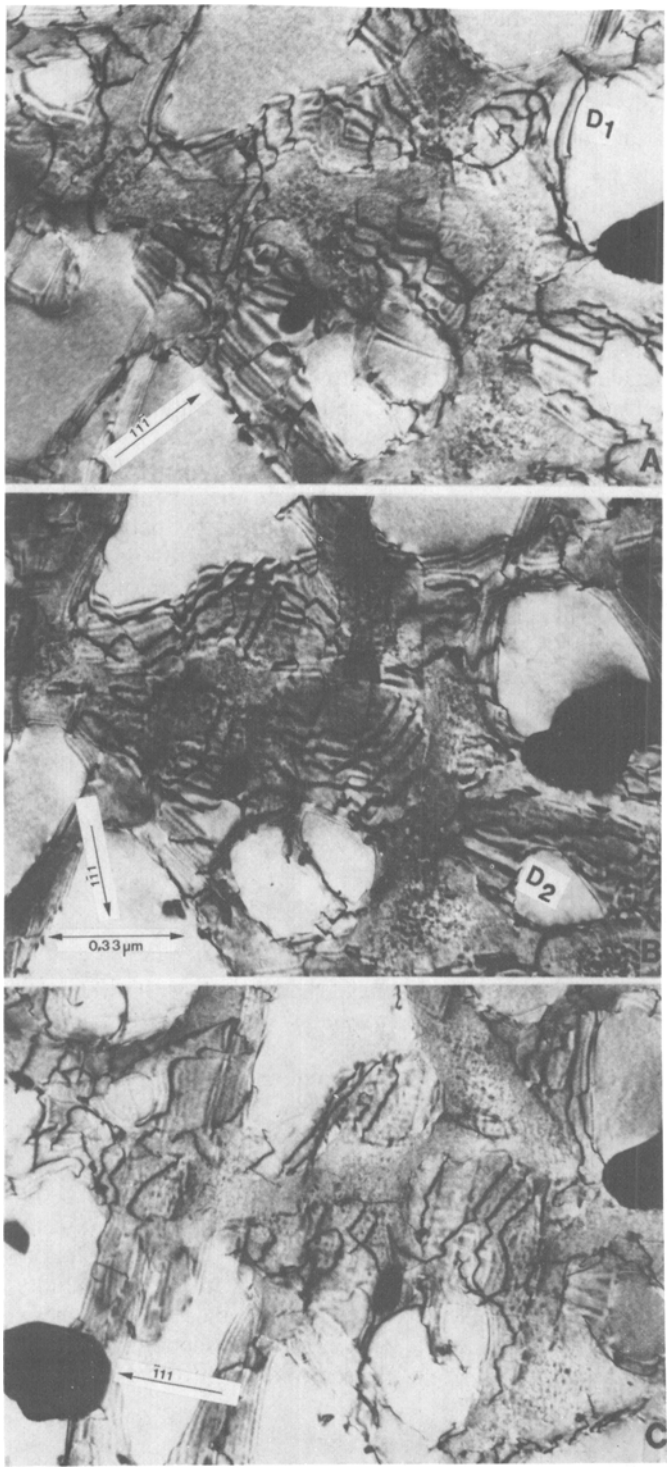

Fig. 1—(*a*, *b*, *c*) show transmission electron micrographs of the same area in three different diffracting conditions: $g = 11\bar{1}$, $1\bar{1}1$, and $\bar{1}11$. D_1 and D_2 are examples of interfacial dislocations.

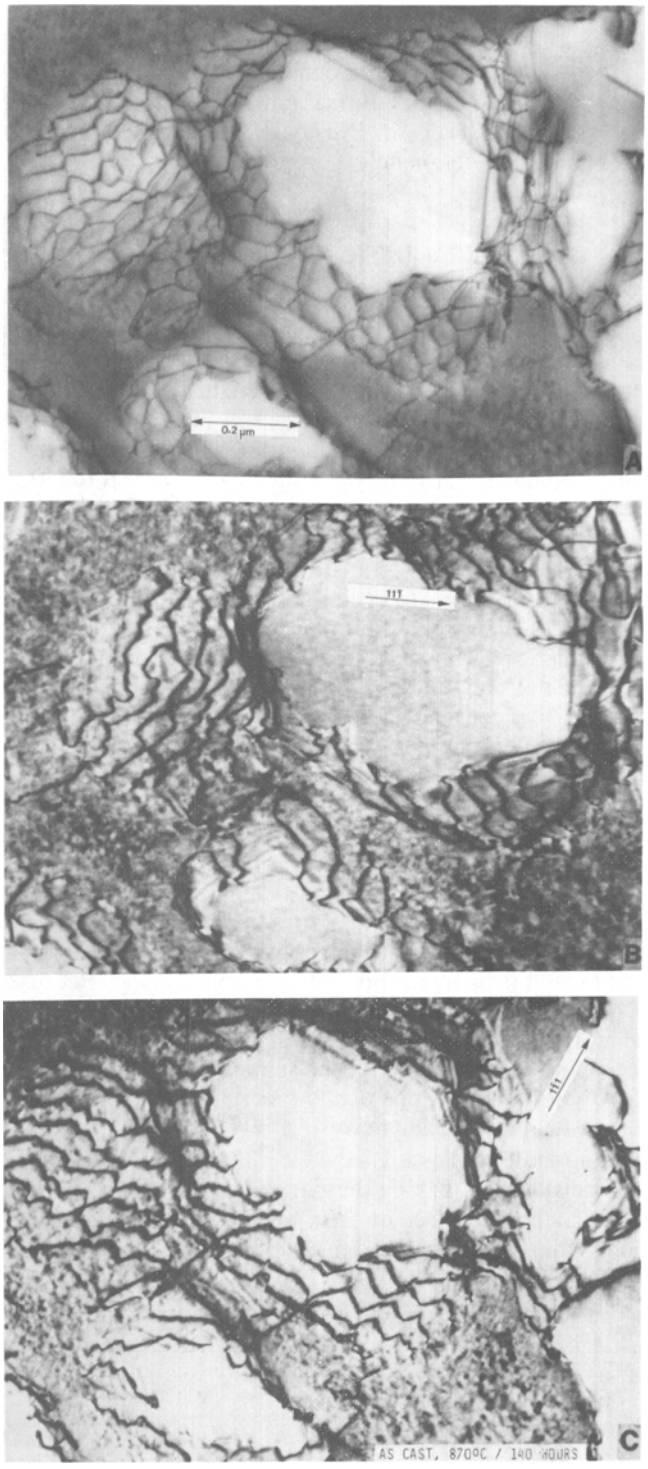

Fig. 2—(*a*) Transmission electron micrograph showing complete network of dislocations. (*b*) and (*c*) are the micrographs of the same area with $g = 11\bar{1}$ and $g = 1\bar{1}1$.

same area using three operating $(11\bar{1}$, $1\bar{1}1$, and $\bar{1}11)$ **g** vectors, respectively. Invisibility criteria for the dislocations $(\bar{g}.\bar{b}. = 0)$ can be readily found from Table II.

Examination of Table II indicates that the dislocations in Figure 1 are of $a/2\langle 110\rangle$ type Burgers vector. Some reflections other than $\langle 111\rangle$ type were also used to confirm $a/2\langle 110\rangle$ type Burgers vector. Each dislocation is visible for two $\langle 111\rangle$**g** vectors and invisible for the third. For clarification dislocations on interfaces are marked as D_1 and D_2. In addition, the figures indicate that the dislocations are predominantly of edge character. This can be easily ascertained from the fact that where the dislocations are invisible, their line vectors are parallel to one of the $\langle 111\rangle$ **g** vectors while their Burgers vectors are perpendicular to that **g** vector.

Figures 2(a), (b), and (c) show the micrograph under multibeam and two beam conditions. Unlike Figure 1, Figure 2 shows the complete network of dislocations at the γ/γ' interfaces. Figures 2(b) and 2(c) show the same area for $\mathbf{g} = [11\bar{1}]$ and $[1\bar{1}1]$, respectively, confirming that all the dislocations in the network are $a/2\langle 110\rangle$ and are of edge type. From these two sets of micrographs, it is clear that the gamma-prime precipitates, which have misfit dislocations, are irregular in shape. Also comparison of Figures 1 and 2 shows precipitates with different degrees of completion of misfit dislocation network. The $a/2\langle 110\rangle$ dislocations in Figure 2 form a complete network. The following conclusions are reached based on the Burgers vector analysis:

(a) Dislocations at interfaces (as well as in matrix) have $a/2\langle 110\rangle$ Burgers vector. Interfacial dislocations are predominantly edge in character whereas dislocations in the matrix are of mixed type.
(b) Gamma-prime precipitates appear to have an irregular morphology when a network of dislocations is present. Those that do not have the network are cuboidal.

Because of small lattice misfit in these superalloys, the stresses at gamma-prime precipitates due to coherency are not expected to be large enough to spontaneously nucleate misfit dislocations, either by shear or by the prismatic punching process.[6] Consistently, no evidence for dislocation nucleation was *seen* near gamma-prime precipitates. Therefore to further analyze evolution of the misfit dislocation network, TEM specimens were prepared after different aging times as indicated below. Some specimens were also examined after creep deformation to evaluate the effect of externally imposed strains. Specific heat treatment conditions were:

(a) solutionized (1225 °C) and water quenched;
(b) solutionized, quenched, and aged for 2 hours at 1000 °C;
(c) solutionized, quenched, and aged for 8 hours at 1000 °C;
(d) conventionally heat treated as-cast specimens that were creep tested at 870 °C and 25 ksi to various strains, namely, 0.25 pct, 1 pct, and rupture (>~5 pct).

B. *Dislocation Network Formation during Aging*

Transmission electron microscopy of as-quenched specimens reveals that gamma-prime is cuboidal. Gamma-gamma prime interfaces are fully coherent, since they are devoid of any misfit dislocations and are of {100} type (*i.e.*, the {100} plane of gamma-prime precipitates is parallel to the {100} plane of gamma). In addition to gamma and gamma-prime, MC and $M_{23}C_6$ carbides are present. Identification of these phases was carried out using electron diffraction techniques. The density of $M_{23}C_6$ type carbides is far less in quenched specimens. Dislocations in the matrix are rarely observed.

Figures 3(a) and (b) present electron micrographs of specimens aged for 2 hours. Figure 3(a) shows the presence of gamma, gamma-prime, MC, and $M_{23}C_6$ as well as dislocations. Note that the dislocations (in matrix) are all

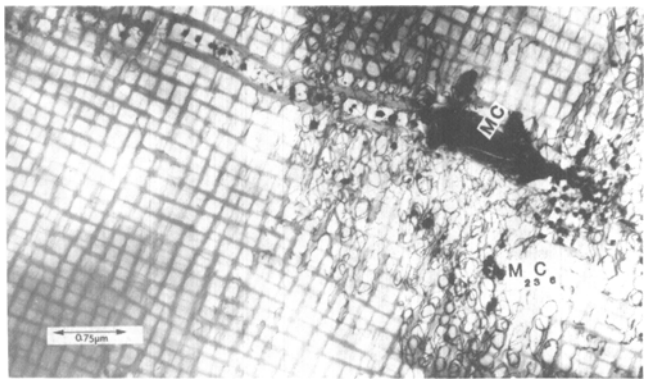

(*a*)

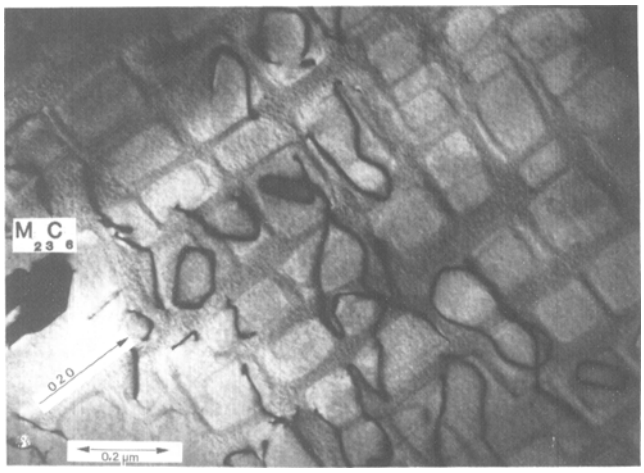

(*b*)

Fig. 3—(*a*) Transmission electron micrograph of specimen aged for 2 h at 1000 °C showing γ, γ', MC, $M_{23}C_6$ carbides, and dislocation loops. Notice that dislocations avoid gamma-prime. (*b*) Another example of the same specimen showing dislocation loops.

Table II. $\bar{g}.\bar{b}.$ Analysis

$\bar{g}/\bar{b}$	½[1$\bar{1}$0]	½[10$\bar{1}$]	½[0$\bar{1}\bar{1}$]	½[110]	½[101]	½[011]
11$\bar{1}$	0	1	1	1	0	0
$\bar{1}$11	1	0	1	0	1	0
$\bar{1}\bar{1}\bar{1}$	1	1	0	0	0	1

$\bar{g}.\bar{b}. = 0$ invisible
$\bar{g}.\bar{b}. = 1$ visible

confined to an area near the carbides (again in the matrix) and are all of the $a/2\langle 110\rangle$ type. They are nucleated near the carbides due to a large lattice mismatch of the carbides with the matrix gamma phase and the consequent large internal stresses generated when carbides precipitate during aging. Note that the misfit dislocation network formation is not complete after 2 hours of aging and many precipitates are still devoid of misfit dislocations. Further note that there is no dislocation generation at the gamma-prime precipitates themselves. Instead, Orowan loops are formed by the passage of itinerant dislocations.

The first stage in the Orowan loop formation can be seen more clearly in Figure 4(a). As the matrix dislocations bypass the precipitates, they leave behind an irregular hexagonal loop around the precipitate (the intersection of a (111) glide plane with a (100) cuboidal precipitate is either a triangle or an irregular hexagon as shown schematically in Figure 4(b)). Segments of such loops formed in close proximity to precipitate corners can cross slip or climb along the interface to form roughly rectangular loops of predominantly edge character. Such rectangular loops with segments parallel to $\langle 110\rangle$ directions can be seen in both Figures 3(b) and 4(a). These loops could collapse by climb. Thus the formation of Orowan loops and subsequent cross slip and climb along the interface would represent the initial steps in the formation of a misfit dislocation network.

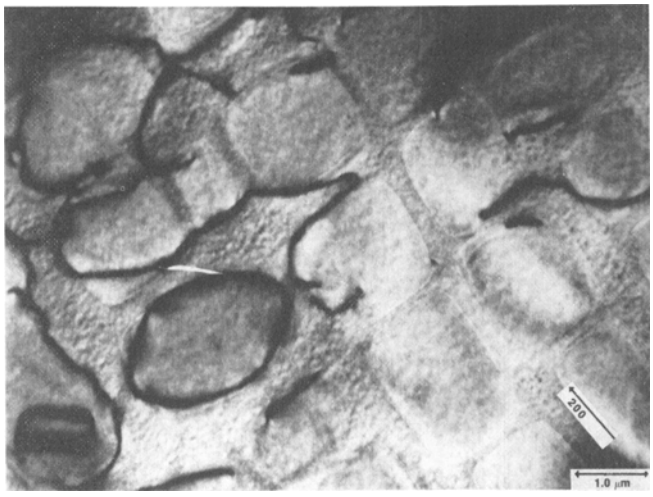

(*a*)

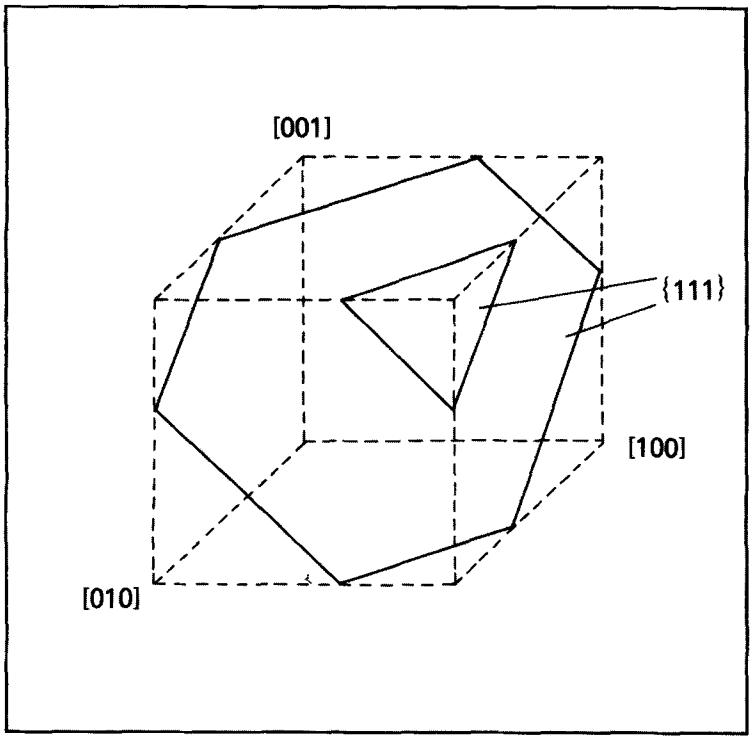

(*b*)

Fig. 4—(*a*) Transmission electron micrograph showing an Orowan loop and the dislocation squeezing between gamma-prime precipitates. (*b*) Schematic diagram of hexagonal and triangular Orowan loops formed by the glide of dislocations on (111) planes (around cuboidal gamma-prime precipitates).

Figures 5(a) and (b) are characteristic of a specimen aged for 8 hours at 1000 °C. This micrograph is taken in (100) orientation. Notice significant coarsening of gamma-prime precipitates during 8 hours of aging and also their irregular shape. Most of the γ/γ' interfaces are no longer parallel to {100} planes. Figure 5 clearly shows long, straight dislocations which lie at the interface. Presence of these dislocations and the change in the orientation of the interface plane from {100} are closely interrelated. A few dislocations in the matrix may also be noted. In addition, dislocations in the matrix near the carbides can be observed. Although there are a number of dislocations at the precipitate inter-

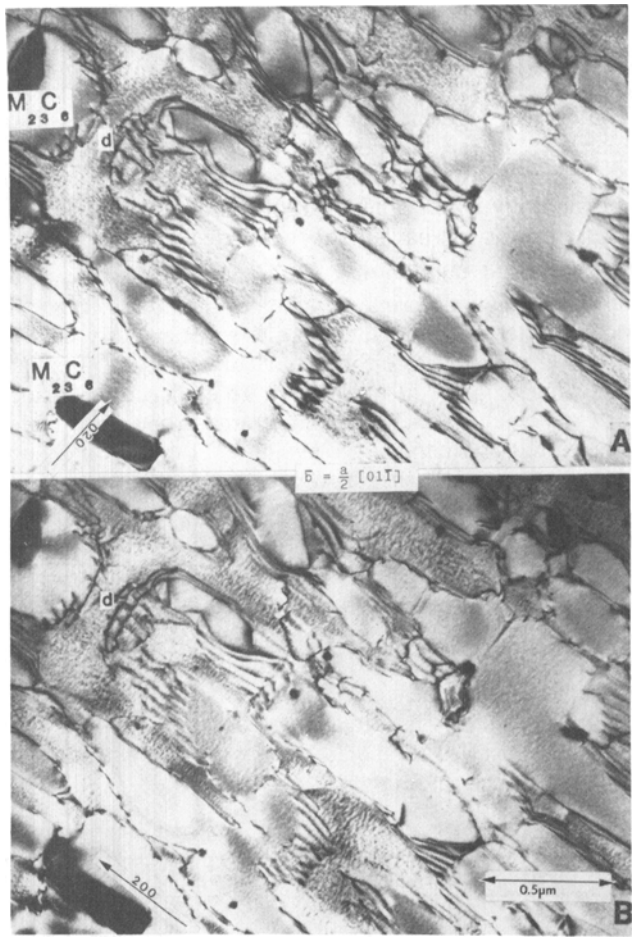

Fig. 5—(*a, b*) Transmission electron micrographs of the same area of the specimen aged for 8 h at 1000 °C. Specimen orientation is (001). Notice the change of orientation of gamma and gamma-prime interfaces through diffusion.

faces, a complete network has not yet formed even after 8 hours of aging.

In summary, as the dislocations generated through the internal stresses near carbides glide and bypass γ'-precipitates, they leave Orowan loops which undergo cross slip and climb to form misfit dislocation loops. As these dislocations accumulate, the planes that define the interface also begin to change.

C. *Dislocation Network Formation after Creep*

Figures 6(a), (b), and (c) illustrate the dislocation structure developed at different strains during creep. Figure 6(a) shows micrographs at low strain where the density of dislocations in the matrix is high. Figures 6(b) and (c) show micrographs at higher strain revealing dislocations at interfaces. These results show that interfacial dislocation formation is accelerated during creep. In this case significant morphological changes occurred with the result that the original {100} interface plane between gamma and gamma-prime is completely altered. Analysis again shows that glide dislocations from the matrix leave behind Orowan loops which undergo cross slip and climb to form misfit dislocation networks. No shearing of the precipitates occurs at this temperature for the stresses imposed.

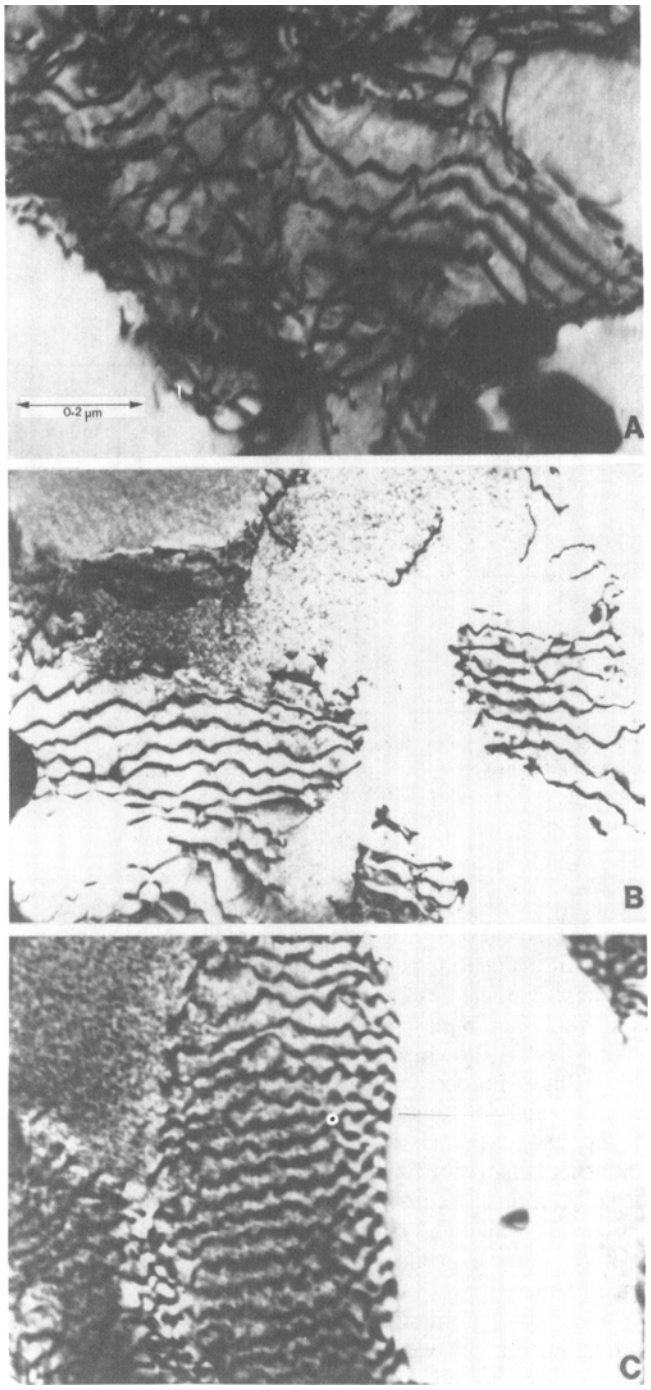

Fig. 6—(*a*, *b*, *c*) Transmission electron micrographs of creep tested specimen at 0.25 pct, 1 pct, and 5 pct strains.

III. DISCUSSION

In the light of the present results, it is instructive to examine current theories of the formation of misfit dislocations around precipitate particles. For a simple case of the two-phase boundary, shown in Figure 7(a), the lattice misfit between the two phases can be described by a parallel array of edge type interfacial dislocations (shown dotted) associated with each interatomic spacing in which the Burgers vector of each interface dislocation is given by $b_I = a - b$. The boundary is essentially coherent with long range stress field arising from this interfacial dislocation array. In the terminology of Bollmann these dislocations can be uniquely defined by a DSC lattice.[7] To reduce the long range stresses generated by the array, crystal lattice dislocations of Burgers vector b_L can be introduced into the boundary, reducing the boundary to semicoherent or incoherent, as shown in Figure 7(b). In this process crystal lattice dislocations, normally referred to as misfit dislocations, need to be nucleated in the form of loops where one half of each is attached to the boundary to compensate for the misfit while the other half is repelled into the matrix (or particle).

When one considers the growth of a spherical precipitate particle from its nucleus, the particle is initially fully coherent with coherency stresses related to the distribution of edge type of dislocation loops represented schematically in Figure 7(c). The loops expand as the particle grows with the stress field proportional to a^3/R^3 where a is the radius of the particle and R is the distance from its center. To form a misfit dislocation completely around the particle, a prismatic loop first needs to be nucleated which can expand by climb into two concentric loops leaving an inner loop around the particle while the outer one expands into the matrix. The sequence of operation can be represented schematically in Figures 7(d), (e), and (f).[8] Alternatively, shear loops can nucleate near the particle which subsequently cross slip to form prismatic loops. The sequence of the process is shown in Figures 7(g), (h), and (i).[8] Note that this process also generates two prismatic loops and that one loop is attracted to the particle to form a misfit dislocation loop while the other one is repelled into the matrix. The loop that is dispersed into the matrix carries the net change in volume expressible as excess interstitials or vacancies which need to be dissipated to dislocations, grain boundaries, or free surfaces. This volume change becomes significant for large volume fraction of precipitates when they become partially or fully incoherent.

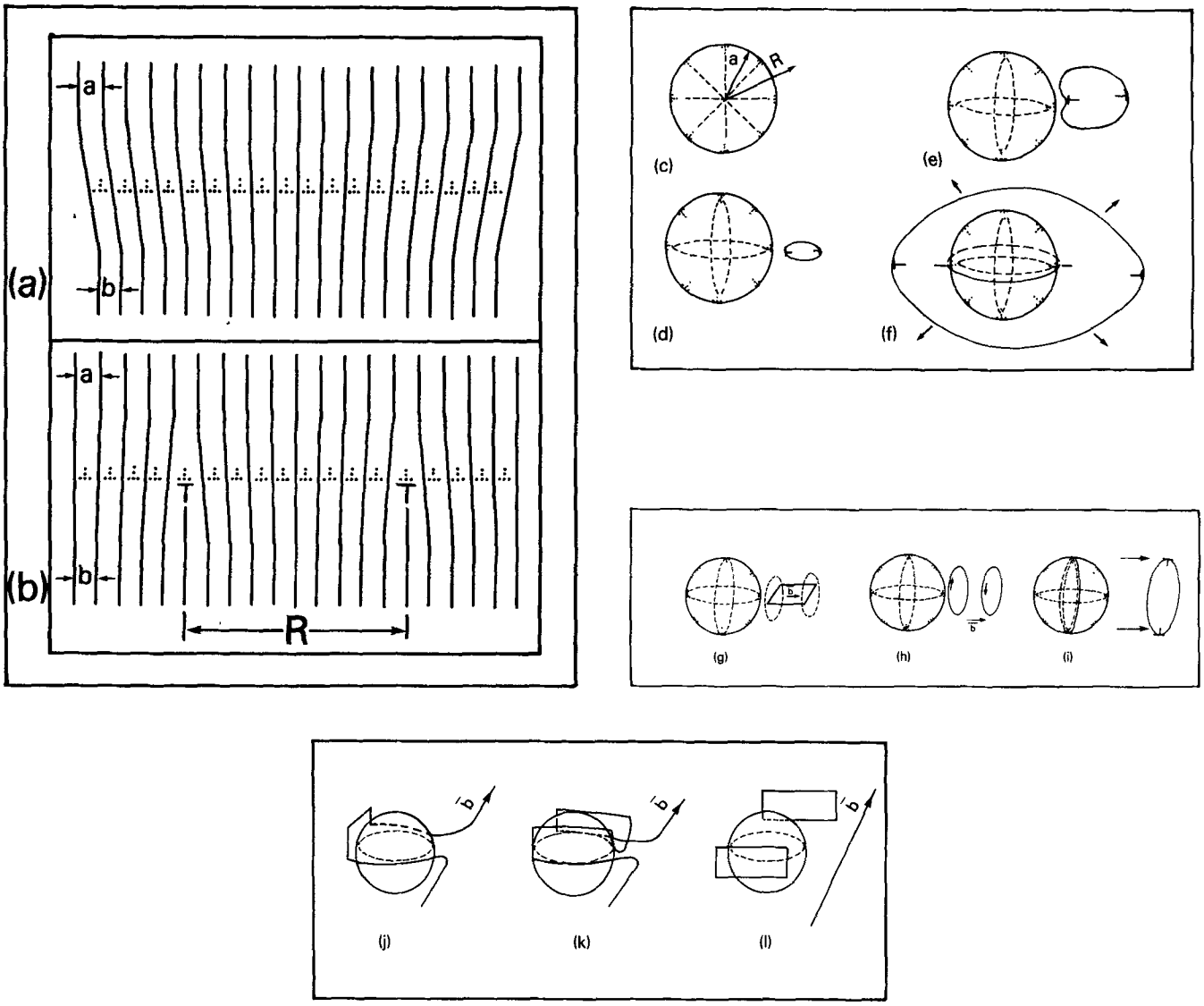

Fig. 7—(*a*) Schematic diagram showing coherent interface; (*b*) illustrates the relief of coherency strain by dislocations. (*c, d, e, f*) Schematic of the evolution of a shear loop near spherical precipitate and its incorporation as misfit dislocation around precipitate. (*g, h, i*) illustrate the process of prismatic punching. One dislocation loop is attracted toward the precipitate to accommodate misfit while the other is repelled. (*j, k, l*) show the formation of two prismatic loops on the precipitate *via* cross-slip of screw dislocation.

For the nucleation of a loop at the precipitate interface, the stresses at the particle must be sufficiently high. Weatherly has found that to nucleate a dislocation loop at a precipitate interface would require a stress greater than $\mu/35$, which is of the order of the theoretical stress.[6] In terms of Eshelby's terminology, this requires a critical dilation strain[6] of e^T equal to 0.04. For the superalloy IN 713C, the lattice mismatch δ is about 0.003 or less. Here $\delta = 2[(a_1 - a_2)/(a_1 + a_2)]$ where a_1 and a_2 are, respectively, the lattice parameters of precipitate and matrix. For IN 713, the lattice mismatch results in e^T of 0.009, which is significantly less than that required for the spontaneous nucleation of a dislocation loop. Experimental observations, in fact, confirm that no dislocation generation occurs at gamma/gamma-prime interfaces. On the other hand, the lattice mismatch δ for $M_{23}C_6$ carbides is about one, resulting in significantly large internal stresses in the vicinity of these carbides. Therefore, dislocation loops are nucleated spontaneously, and these expand and multiply, generating dislocations in the matrix. These itinerant or matrix dislocations then provide sources for the generation of misfit dislocations around gamma-prime particles.

These dislocations can generate prismatic loops by cross slip when they bypass a particle as originally suggested by Ashby and as shown schematically in Figures 7(j), (k), and (l).[8] But this process actually leads to two prismatic loops, one of which is attracted by the precipitate, while the other is repelled and needs to be dissipated into the matrix. All the mechanisms for formation of misfit dislocations which have been discussed above and which have been observed in certain selected systems appear to be inapplicable to gamma/gamma-prime systems, probably because of low misfit strain.

An analysis of misfit dislocation network around gamma-prime precipitates was made previously by Lasalmonie and Strudel (LS),[5] and they concluded that three sets of independent ⟨110⟩ Burgers vectors are required to form a complete network. In particular, they considered a precipitate in

the shape of tetrakaidecahedron[3] (Figure 8) consisting of eight [111] and six [100] planes and showed that a complete network of pure edge dislocations can be formed using three independent ⟨110⟩ Burgers vectors. Mutual interaction of these dislocations results in a hexagonal network, involving three Burgers vectors on {111} planes and an orthogonal network involving two Burgers vectors on {100} planes. The selection of the shape of the particle is such that for any segment of each loop on any particular plane, both the line vector and Burgers vector lie in that plane. Although the authors do not state so explicitly, satisfying this condition results in maximum misfit accommodation and, accordingly, maximum reduction in the misfit energy. This is an important consideration in misfit dislocation network formation. But for a cuboidal particle, although three sets of ⟨110⟩ Burgers vectors may still be needed to form a complete network, both Burgers vectors and line vectors of all segments of all loops do not lie on their respective planes. In such circumstances the shape of the particle will tend to change.

The present results show that all of the observed dislocations around gamma-prime precipitates are of ⟨110⟩ type Burgers vectors and are of predominately edge character, in agreement with LS analysis. What remains to be accounted for are the sources for the prismatic dislocation loops, the energetics for the formation of prismatic loops from glide loops, and the modification of the shape of the particles. The present analysis addresses each of these missing links.

Regarding the source of dislocations, in the case of creep-specimen deformation, dislocations produced by the external stress provide the loops required for the network. For the unstressed aged specimen, internal stresses arising from carbides provide sources. Thus, misfit network formation is homogeneous throughout the specimen and occurs readily during creep while it is localized and occurs only after prolonged aging in unstrained specimens.

For creep specimens, imposed external stresses provide the required driving force to squeeze the dislocations through the interstices between the particles. For the unstressed aged specimen, stress fields of the carbides fall off rapidly as a^3/R^3, where a is the radius of the carbide particle and R is the distance from the center of the particle. The additional driving force for glide and climb is provided by the coherency stresses surrounding gamma-prime. For the high volume fraction of gamma-prime normally encountered in superalloys, the three dimensional alignment of the

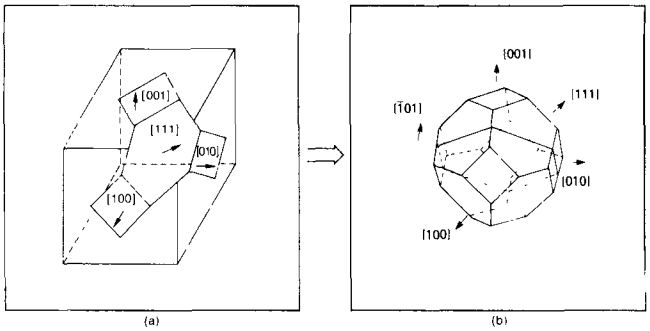

Fig. 8—Change in the shape of a cuboidal gamma-prime. (*a*) Rounding of the corners to form a {111} facet. (*b*) Final shape (tetrakaidecahedron).[5] Interfaces are of {111} and {100} type. A pure edge dislocation loop with $a/2$[101] is shown.

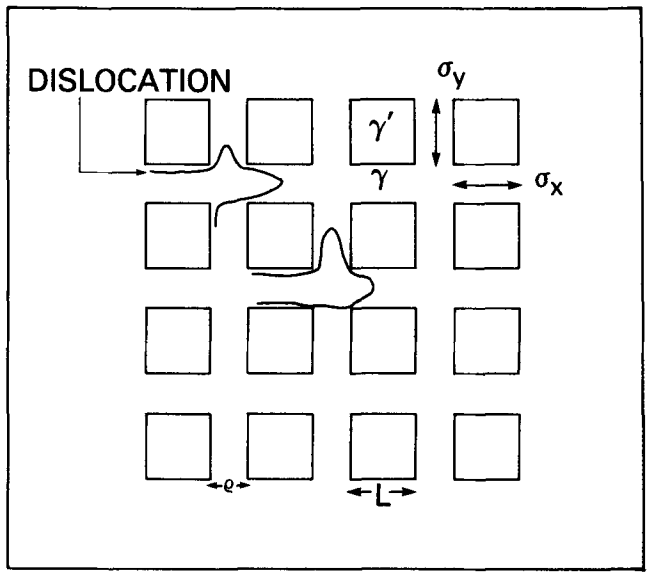

Fig. 9—Schematic illustration of the biaxial stresses between cuboidal gamma-prime precipitates and the passage of itinerant dislocations in the gamma phase.

particles along cube directions shown schematically in Figure 9 results in biaxial stresses[9] given by

$$\sigma = \frac{L\delta E}{(\rho + L)} \qquad [1]$$

where L is the size of the particle, ρ is the spacing between the particles, δ is the lattice misfit, and E is the Young's modulus. For simplicity we ignore the difference in moduli between the two phases and consider only the changes in volume as the precipitation occurs.

As the dislocations bypass the particles as a result of the above stresses, Orowan loops are formed, as observed in Figure 5. These glide loops can, by virtue of the stress fields present, rotate by cross slip and climb into prismatic configuration, and this is shown schematically in Figures 10(a), (b), and (c). Note that the opposite edge segments of the loop climb in opposite directions, thereby contributing to the net flux of vacancies or interstitials. A flux of vacancies is equivalent to a counter current of matter. of matter.

The net climb distance for each loop as it rotates to form a prismatic dislocation is equal to the size of the particle, as shown by simple geometry in Figure 10(d). The net climb of dislocation segment A is AC-DE, and that of segment F is FH-IJ, which from the geometry are equal to

$$AB + FG = EJ = L$$

where L is the size of the particle.

The driving force for the rotation of the glide loop into a prismatic loop can be determined by considering the total energy of the system before and after the rotation. The strain energy inside the particle before rotation is simply given by

$$E_p = \frac{1}{2}\frac{\sigma_p^2 L^3}{K} \qquad [2]$$

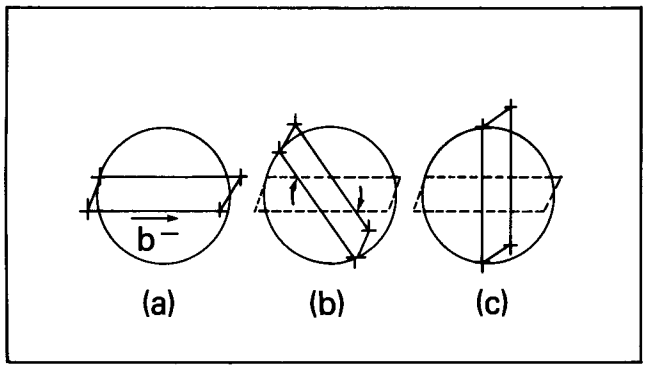

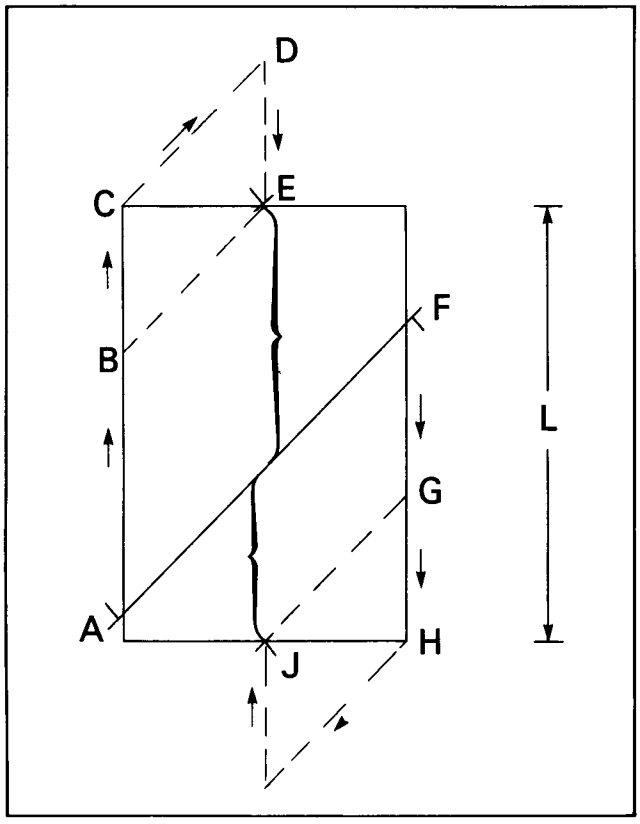

(*d*)

Fig. 10—(*a*, *b*, *c*) show the rotation of a glide loop to become prismatic. (*d*) Schematic illustration showing the net climb of the edge segments of a dislocation loop is equal to the cross-sectional area of the precipitate.

where σ_p is the stress inside the particle of size L and K is the bulk modulus. The stress σ_p is given in terms of lattice misfit δ by

$$\sigma_p = \frac{\rho\delta E}{(\rho + L)} \qquad [3]$$

Likewise the stored elastic energy in the matrix before rotation is given by

$$E_m = \frac{1}{2}\frac{\sigma_m^2 3L^2\rho}{E} \qquad [4]$$

where σ_m is the stress in the matrix in between particles, ρ is the spacing between the particles, and E is the Young's modulus. From equilibrium considerations

$$\sigma_m = \frac{\sigma_p L}{\rho} \qquad [5]$$

The total energy is then given by

$$E_T = E_p + E_m = \frac{1}{2}\frac{\rho^2}{(L+\rho)^2}\delta^2 E^2\left(\frac{L^3}{K} + \frac{3L^4}{\rho E}\right). \qquad [6]$$

When prismatic dislocation loops form, misfit δ is relieved and, therefore, the change in energy with change in δ is

$$\frac{dE_T}{d\delta} = \frac{\rho^2}{(L+\rho)^2}\delta E^2\left(\frac{L^3}{K} + \frac{3L^4}{\rho E}\right). \qquad [7]$$

Three mutually perpendicular loops contribute to a reduction in δ by amount b/L where b is the magnitude of the Burgers vector. The net change in energy per dislocation as a result of its rotation is

$$\Delta E = \frac{\rho^2\delta b E^2}{3(L+\rho)^2}\left(\frac{L^3}{K} + \frac{3L^4}{\rho E}\right) \qquad [8]$$

As shown in Figure 10(c), each dislocation loop climbs a distance of L during its rotation and, therefore, the net driving force for climb for each loop is

$$\frac{\Delta E}{L} = \frac{\rho^2\delta b E^2}{3L(L+\rho)^2}\left(\frac{L^3}{K} + \frac{3L^4}{\rho E}\right) \qquad (9)$$

As each loop rotates, δ is reduced and the driving force for the subsequent loops decreases. It would fall to zero if all the misfit were accommodated.

As the Orowan loops rotate into prismatic loops, the process is accompanied by the diffusive transport of matter of volume L^2b to and from the particle surface, with another particle interface, dislocation, grain boundary, or free surface acting as a source or sink to compensate. This matter transport permits a change in shape of the particle from cuboidal to possibly tetrakaidecahedral, as pictured by the LS model, where each dislocation loop accommodates maximum misfit. Figures 1 and 2 show many precipitates with rounded corners. Change in the morphology can therefore occur starting from corners, resulting in the formation of {111} facets. Figure 8(a) shows schematically the formation of a facet at one of the corners of the cube. Tetrakaidecahedral shape with eight {111} and six {100} facets, as indicated in Figure 8(b), can form eventually with the formation of the complete network of ⟨110⟩ prismatic dislocations. As stated earlier, because of this shape, any ⟨110⟩ loop segment on any particular plane has both line vector and Burgers vector on that plane. This provides a maximum misfit accommodation. Viewed differently, relief of misfit may be thought of as reduction in surface energy, where, in order to decrease surface energy, precipitates tend to become spheroidal. In fact, in superalloys where misfit is essentially zero, gamma-prime forms as spheroidal rather than cuboidal precipitates.

In summary, the sequence of network formation involves the glide of dislocations in the matrix generated as a result of internal stresses during carbide precipitation (or external stress during creep) which form Orowan loops as they bypass the gamma-prime precipitates. These glide loops rotate into prismatic configuration by cross slip and climb. In fact, such rotations of glide loops have also been ob-

served experimentally[10] through high voltage electron microscopy. Dislocation interactions as discussed in the LS analysis can now occur, resulting in a complete three dimensional network of misfit dislocations. As the climb involves a net transport of matter, this enhanced diffusion allows a change in morphology of the precipitates, as observed experimentally.

IV. CONCLUSIONS

In nickel base superalloys gamma-prime loses its coherency with prolonged aging or by plastic deformation. Dislocations at the interfaces are of $a/2\langle 110\rangle$ type with predominantly edge character.

During aging, dislocations are generated through internal stresses arising from the precipitation of carbides. These dislocations glide because of biaxial stresses produced in the presence of a high volume fraction of gamma-prime precipitates. As the dislocations bypass the precipitates, they leave behind Orowan loops. These rotate into prismatic loops by combined cross slip and climb. To maximize the misfit accommodation, the morphology of the precipitates changes from a cubic one to tetrakaidecahedral form in which each segment of the prismatic dislocations has its Burgers and line vectors parallel to the plane of the interface.

REFERENCES

1. Thomas G. Ference and Samuel M. Allen: *Metall. Trans. A*, 1986, vol. 17A, pp. 2239-47.
2. C. Carry and J. L. Strudel: *Acta Metall.*, 1980, vol. 26, pp. 859-70.
3. C. Carry and J. L. Strudel: *Acta Metall.*, 1977, vol. 25, pp. 767-77.
4. G. C. Weatherly and R. B. Nicholson: *Phil. Mag.*, 1968, vol. 17, pp. 801-31.
5. A. Lasalmonie and J. L. Strudel: *Phil. Mag.*, 1976, vol. 32, pp. 937-49.
6. G. C. Weatherly: *Phil. Mag.*, 1976, vol. 32, pp. 791-99.
7. W. Bollmann: *Crystal Defects and Crystalline Interfaces*, Springer-Verlag, New York, NY, 1970.
8. J. W. Mathews: *Dislocations in Solids*, F. R. N. Nabarro, ed., 1979, vol. 2, pp. 6161-545.
9. N. Louat, K. Sadananda, and M. A. Imam: *Structure and Deformation of Boundaries*, The Metallurgical Society, Inc., 1985, pp. 299-316.
10. F. J. Humphreys and V. Ramaswamy: *Proc. 3rd Int. Conf. High Voltage Electron Microscopy*, P. R. Swan, C. J. Humphreys, and M. J. Goringe, eds., 1974, pp. 268-72.